Tutor/s

Dra. Anna Maria Costa Arnau
Departament de Química Orgànica

Dott.ssa Elisa Viola
Sapienza University of Rome

Grau de Química

Treball Final de Grau

Non-Covalent Functionalization of Graphene Oxide with Porphyrazine Macrocycles

Funcionalització No Covalent de l'Òxid de Grafè amb Macrocicles de Porfirazina

Pol Pérez Quer

Juliol 2023

Universitat de Barcelona

B:KC Barcelona Knowledge Campus
Campus d'Excel·lència Internacional

Science knows no country because knowledge belongs to humanity, and is the torch which illuminates the world.

Louis Pasteur

I would like to express my heartfelt gratitude to the following individuals who have contributed significantly to the completion of this thesis:

Dr. Elisa Viola, my Host tutor, for her warm welcome, encouragement, and provision of essential resources during my time at the host university. Her mentorship and encouragement have been invaluable in expanding my knowledge and skills.

Dr. Anna Maria Costa, my home tutor, for her unwavering support, guidance, and invaluable insights throughout the research process. Her expertise has been instrumental in shaping the direction of this work.

Dr. Mauro Giustini for generously providing the necessary instruments for this thesis while offering me guidance on the interpretation of the recorded spectra, enhancing my understanding of the results. His support and assistance in accessing these vital resources are greatly appreciated.

Dr. Francesco Amato, my lab supervisor, for his expert supervision, continuous guidance, and patience. His insightful feedback and technical expertise have greatly enhanced the quality of this research.

I would also like to extend my gratitude to my dedicated lab partners, **Lorys Di Nardi** and **Giorgia Marcaurelio**. Their collaboration, enthusiasm, and shared commitment to excellence have made the research journey both enjoyable and rewarding.

Lastly, I would like to acknowledge the support of my friends and family who have provided me with encouragement, understanding, and a nurturing environment throughout this endeavor. Their unwavering belief in my abilities has been a constant source of motivation.

REPORT

IDENTIFICATION AND REFLECTION ON THE SUSTAINABLE DEVELOPMENT GOALS (SDG)

In light of the information provided, this project's impact for the achievement of the Sustainable Development Goals (SDGs) can be primarily linked to two main areas:

People: The project's core focus on developing a porphyrazine-graphene oxide hybrid material for potential biomedical applications, particularly in Photodynamic Therapy, directly aligns with SDG 3 (Good Health and Well-Being). By aiming to contribute to overall well-being through innovative cancer treatment methods, the project supports the goal of ensuring good health and well-being for all. It can also be linked to SDG 4 (Quality Education) by contributing to expanding knowledge and understanding in the field of photosensitizers, specifically porphyrazine-graphene oxide hybrids. This knowledge dissemination can support quality education initiatives and promote scientific advancements in related fields.

Prosperity: The successful synthesis and characterization of the porphyrazine-graphene oxide hybrid material can contribute to prosperity through economic growth. The development of novel nanomaterials and their potential applications create opportunities for innovation, employment, and economic advancement, aligning with SDG 8's objective of fostering decent work and sustainable economic growth.

By recognizing the project's alignment with these Sustainable Development Goals, we gain a deeper understanding of its potential impact on various dimensions of sustainable development. This identification allows us to reflect on the project's contributions, explore synergies with the SDGs, and pave the way for future investigations and applications with the aim of advancing sustainable development in relevant fields

CONTENTS

1. SUMMARY

Graphene Oxide (GO) possesses a large and rigid π-conjugated planar structure, coupled with oxygen-containing groups on the edges and in the basal plane, which provides the material with several amazing physicochemical properties, such as excellent water dispersibility, surface modifiability, biological compatibility, and so on. For these reasons, it is considered among the most promising nanomaterials for biological imaging or sensing, drug delivery, composite materials, and luminescent devices.

This report presents a comprehensive study on the non-covalent functionalization of graphene oxide (GO) with a pentanuclear porphyrazine macrocycle (Pz), exactly $[(PtCl_2)_4LZn]$ where L = tetrakis-2,3-[5,6-di(2-pyridyl)-pyrazino]porphyrazinato dianion, an active photosensitizer for $^1O_2$ production, with the aim of obtaining a stable hybrid nanostructure with unique physico-chemical properties.

The primary objective was to achieve the binding of porphyrazine molecules to GO sheets, resulting in the synthesis of a novel porphyrazine-graphene oxide hybrid material (Pz@GO). This system was characterized by UV-Visible, infrared (IR) and Raman spectroscopy and photoluminescence measurements. The hybrid Pz@GO shows better water solubility characteristics than pure porphyrazine, which is of great interest for potential biomedical applications in the field of Photodynamic Therapy and in other multimodal therapies. However, the problematic aspect of water solubility needs to be further optimised.

A preliminary investigation on the photosensitizing efficiency of Pz@GO in the production of the $^1O_2$ was carried out, which highlighted the need to select a suitable method to conduct this type of analysis on this nanostructured material.

All the results obtained in this Thesis Work lay the foundation for future investigations and potential biomedical applications, with the aim of further advancing the understanding and utilization of porphyrazine-graphene oxide hybrids in various fields, including Photodynamic Therapy.

Keywords: Non-covalent functionalization, Graphene oxide, Porphyrazine macrocycles, Photodynamic therapy

2. RESUM

L'òxid de grafè (GO) posseeix una estructura plana gran i rígida conjugada amb π, juntament amb grups que contenen oxigen a les vores i al pla basal, que proporciona al material diverses propietats fisicoquímiques sorprenents, com ara una excel·lent dispersibilitat de l'aigua, modificabilitat superficial, compatibilitat biològica, etc. Per aquests motius, es considera un dels nanomaterials més prometedors per a la imatge o la detecció biològica, el lliurament de fàrmacs, els materials compostos i els dispositius luminescents.

Aquest informe presenta un estudi exhaustiu sobre la funcionalització no covalent de l'òxid de grafè (GO) amb un macrocicle de porfirazina pentanuclear (Pz), exactament [$(PtCl_2)_4$LZn] on L = tetrakis-2,3-[5,6-di(2-piridil)-pirazino]porphyrazinato dianió, un fotosensibilitzant actiu per a la producció d'$^1O_2$, amb l'objectiu d'obtenir una nanoestructura híbrida estable amb propietats fisicoquímiques úniques.

L'objectiu principal era aconseguir la unió de molècules de porfirazina a làmines GO, donant lloc a la síntesi d'un nou material híbrid d'òxid de porfirazina-grafè (Pz@GO). Aquest sistema es va caracteritzar per espectroscòpia UV-Visible, infraroja (IR) i Raman i mesures de fotoluminescència. L'híbrid Pz@GO mostra millors característiques de solubilitat en aigua que la porfirazina pura, que és de gran interès per a potencials aplicacions biomèdiques en el camp de la Teràpia Fotodinàmica i en altres teràpies multimodals. Tanmateix, l'aspecte problemàtic de la solubilitat en aigua s'ha d'optimitzar encara més.

Es va dur a terme una investigació preliminar sobre l'eficiència fotosensibilitzant de Pz@GO en la producció de l'$^1O_2$, que va posar de manifest la necessitat de seleccionar un mètode adequat per dur a terme aquest tipus d'anàlisi sobre aquest material nanoestructurat.

Tots els resultats obtinguts en aquest Treball de Final de Grau posen les bases per a futures investigacions i aplicacions biomèdiques potencials, amb l'objectiu d'avançar encara més en la comprensió i utilització dels híbrids de porfirazina-òxid de grafè en diversos camps, inclosa la teràpia fotodinàmica.

Paraules clau: funcionalització no covalent, òxid de grafè, macrocicles de porfirazina, teràpia fotodinàmica

3. INTRODUCTION

3.1. GRAPHENE OXIDE: THE WATER SOLUBLE GRAPHENE DERIVATIVE

3.1.1. Description and importance

Graphene is the fundamental building block for most of the carbon allotropes. It is a two-dimensional atomically thin layer of carbon atoms attached by sp^2 bonds forming a hexagonal lattice.[1] A particular derivative of graphene, graphene oxide (Figure 1), has drawn the attention of the scientific community around the globe for its particular properties. Graphene oxide (GO) is derived from the chemical oxidation of graphite, resulting in a two-dimensional non-stoichiometric material which maintains the conjugated π-system throughout the layer. It predominantly consists of carbon atoms in sp^2 hybridization and contains various oxygen-based functional groups. The most abundant groups on GO are epoxide and hydroxyl groups, which are primarily found in the basal plane of the graphene sheet. In contrast, carboxyl groups are less common and are mainly located at the sheet's edges. Additionally, a small percentage of carbonyl and phenol-like hydroxyl groups can be found, typically confined to the edges of the GO layer.[2]

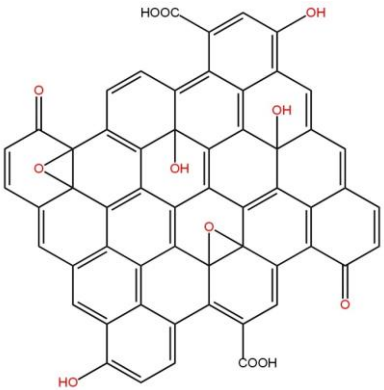

Figure 1. Schematic molecular structure of Graphene Oxide (GO).

The presence of such oxygen-based functional groups makes GO a hydrophilic material and upon sonication in aqueous media it easily exfoliates and forms stable colloidal suspensions. In addition, the incorporation of multiple oxygen-containing groups alters the electrochemical properties of the system and offers enhanced possibilities for further functionalization.

These properties make graphene oxide a very promising material and it has been already studied for numerous applications such as biomolecular sensors, field-effect transistors, graphene batteries and transparent conductive films.[3] Recently, GO have also been considered among the most promising nanocarrier for biomedical applications, due to its fair solubility in water. Unique properties, such as very high surface area, acceptable biocompatibility, and easy surface modification with appropriate functional groups, have great potential for loading hydrophobic drugs and vehiculate them in aqueous medium for advanced drug delivery in the field of various therapies.

3.1.2. Functionalization of graphene oxide

Graphene oxide can be functionalized in a diverse amount of mechanisms that can be categorized into two major groups: covalent and non-covalent functionalization.

Covalent functionalization, as its name suggests, includes all kinds of functionalization that result into a new covalent bond between graphene oxide and the species that is being functionalized with. This is usually done by involving the oxygen containing groups of GO to carry out amidation, esterification, epoxide ring-opening, and silylation reactions. However, covalent functionalization can also target the carbon-carbon bonds of graphene oxide to perform cycloaddition reactions, radical additions or diazotitations.[4]

On the other hand, non-covalent functionalization pursues the successful binding of graphene oxide with the target species without forming a covalent bond. This can be done by overstacking molecules with a conjugated π-system to the graphene oxide surface via π-π stacking or taking advantage of the hydroxyl and carboxyl groups in graphene oxide to retain the target species via ionic interaction or hydrogen bonds. Van der Waals interactions, mainly with species with a high hydrophobic character, also provide a non-covalent functionalization alternative.

3.2. PORPHYRAZINES: PARTICULAR PORPHYRINOIDS

3.2.1. Description and interest

Porphyrazines are synthetic porphyrinoid macrocycles characterized by the presence of a central tetrapyrrolic core with the four pyrrole rings linked together by bridging *meso*- azamethine (-N=) atoms instead of the *meso* =CH- groups present in porphyrins (see "porphyrazine" and "porphyrine" in Figure 2). Their unique optical and electronic properties are the basis of the vast number of researches that study their potentiality for a wide variety of applications including organic electronics, solar energy converters, [5] chemical sensors and liquid crystals among others.[6] Their high absorption between 600 and 700 nm, which is called the *phototherapeutic window*, also makes porphyrazines potential drugs for applications in anticancer phototherapies such as photodynamic therapy (PDT) and photothermal therapy (PTT).[7]

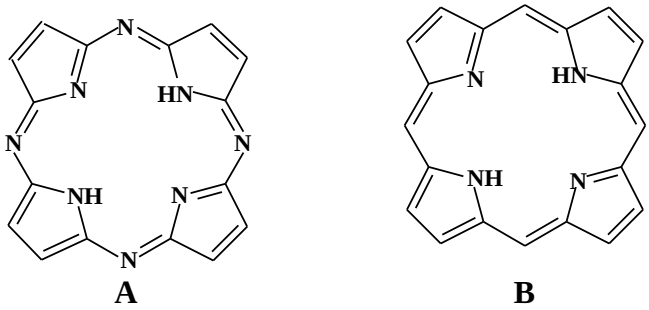

Figure 2. A) Porphyrazine; B) Porphine.

Derivatives from the central porphyrin and porphyrazine cores can be built up in two ways: either by insertion of metal ions by deprotonation of the central NH groups, or by bearing external appropriate substituents on the β-C atoms of the pyrrole rings.[8]

Porphyrazines in general, including phthalocyanines, are normally insoluble in water and show low solubility in low-donor solvents (dimethyl sulfoxide, DMSO; dimethylformamide, DMF; pyridine, py), rarely reaching in these solvents concentrations > 10^{-4} M.[9] Since they have high intensity Soret and Q bands, with ε values of the order of 10^5 cm^{-1} mol^{-1} L, UV-visible spectra can easily be registered using concentrations of the order of 10^{-5}-10^{-6} M, or even lower with adequate instrumentation.

As a representative example of the spectroscopic behaviour of porphyrazines, the UV-visible spectrum of [PcZn] in pyridine solution is shown in Figure 4. The spectrum shows intense absorptions in the Soret region (300-450 nm) (*B* in Figure 4) and in the Q-band region (600-700 nm) (*Q* in Figure 4). In the absence of aggregation, as is the case for [PcZn] in Figure 4, the Q band at 674 nm appears narrow and sharp and clearly indicates that [PcZn] is present in solution essentially in its monomeric form. Aggregation is due to π-π interaction between two or more molecules and can determine limited or quite evident broadening for the Q band. In case of the presence of two distinct absorptions in the Q-band region, this might suggest a monomer/dimer equilibrium which needs to be studied as a function of the concentration, in order to achieve information about the relative stability of the two forms. For these problematic aspects and others related to problems of stability of the monomeric species with the time or reactivity in general, UV-visible spectral studies represent an excellent scientific instrument of investigation.

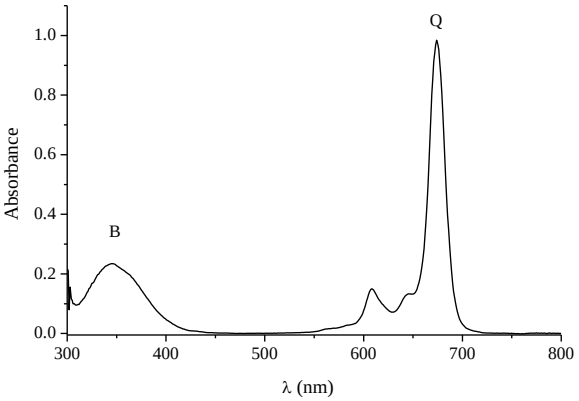

Figure 4. UV-visible spectrum of [PcZn] in

The intense UV-visible absorptions in the Soret and Q-band regions are assigned as due to $\pi \rightarrow \pi^*$ intraligand transitions. Assignment of these transitions can be made based on the energy level diagram proposed by Gouterman[10] (four orbital model; Figure 5) for the porphyrin

macrocycles but then made applicable also to the phthalocyanine and porphyrazine systems. Such diagram easily allows to identify the HOMO-LUMO transitions for [PcM] compounds and also for [PcH_2], and in general for the parent porphyrazine species. As can be seen, the lowering of the symmetry for the change [PcM] (D_{4h} symmetry) $\rightarrow$ [PcH_2] (D_{2h} symmetry) implies the splitting of the two e_g orbitals, which means that for [PcH_2] or a related porphyrazine free-base, [PzH_2], the Q band might be seen as split into two bands named Q_x and Q_y. Depending on the Q_x-Q_y energy separation, the splitting of the Q band can be evidenced by the spectrum or not, this depending also by the type of solvent used.

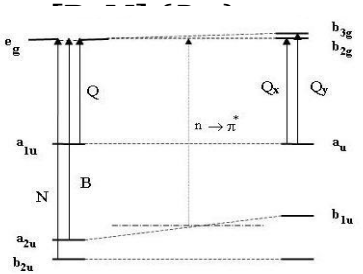

Figure 5. Gouterman orbital energy level diagram of the tetrapyrrolic Pc/Pz macrocycles.

3.2.2 The porphyrazine complex [$(PtCl_2)_4$LZn]

In a recent paper[9], Maria Pia Donzello et al. presented an extensive characterization of novel heteropentanuclear pirazinoporphyrazines with peripherally inserted cisplatin-like functionalities with formula [$(PtCl_2)_4$LM], where L = tetrakis-2,3-[5,6-di(2-pyridyl)-pyrazino]porphyrazinato dianion and M = Zn^{II}, $Mg^{II}(H_2O)$, Pd^{II}, Cu^{II} or Co^{II} (Figure 6).

In these systems, external $PtCl_2$ coordination occurs on a porphyrazine macrocycle characterized by the presence of four dipyridinopyrazine moieties annulated to the pyrrole rings of the central core. An extensive physico-chemical characterization including experimental (UV-vis, NMR, electrochemical) and theoretical (DFT and TD-DFT) studies, reported in the aforementioned paper, has shown that both the electronegative pyrazine/pyridine N atoms and the peripheral $PtCl_2$-unit coordination make these compounds highly “electron-deficient” systems,

with a resulting increment of the σ/π electron density distribution towards the periphery of the macrocycle.

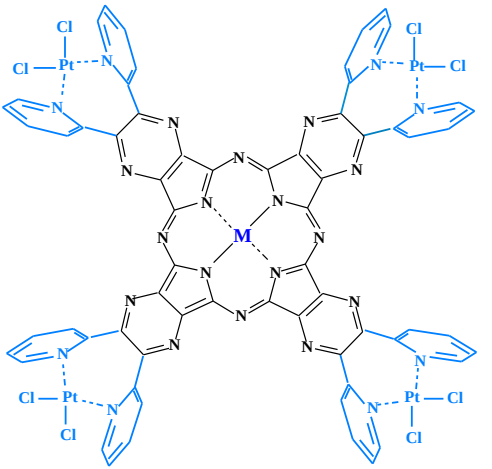

Figure 6. Molecular structure of the porphyrazine complexes $[(PtCl_2)_4LM]$.

Worth of notice, the structural arrangement of the N_2PtCl_2 site has also been investigated by X-ray and NMR combined work on the $PtCl_2$ derivative of the synthetical precursor of the macrocycle, ie $[(CN)_2Py_2PyzPtCl_2]$.[11] The structure of the complex shows a non-coplanar positioning of the pyrazine and pyridine rings. In addition, the $N_{2(py)}PtCl_2$ square planar coordination site lies nearly perpendicular to the plane of the pyrazine ring. This is a privileged basis of structural information on the exocyclic coordination of $PtCl_2$ units in the octapyridinated pyrazinoporphyrazine macrocycle.

It was proved that, among the various reported complexes, the pentametallic species $[(PtCl_2)_4LZn]$ is of special interest because it behaves in organic solvent as an excellent photosensitizer for singlet oxygen, $^1O_2$, the main citotoxic agent active in Photodynamic Therapy (see Section 3.3.2), showing a significant value of singlet oxygen quantum yield in DMF (Φ_Δ = 0.52). In addition, the four cis-platin like peripheral functionalities, N_2PtCl_2, closely resemble cis-platin, $(NH_3)_2PtCl_2$, the potent anticancer chemotherapeutic drug used for many years (and still today) to treat a variety of tumors.[12] These combined features provide the complex $[(PtCl_2)_4LZn]$

good potentialities for a bimodal photo-chemotherapeutic antitumor modality, a step forward from PDT which uses a single molecule to achieve a synergistic therapeutic action with reduced overall side effects. Notably, since cis-platin is highly toxic for noncancer cells, its use in association with PDT might lead to a more sustainable therapy.

For all these reasons, the species [$(PtCl_2)_4$LZn] was selected as the object of the investigation for the synthesis of the Pz@GO hybrid material, as will be discussed in section 5.2.

3.3. NON-COVALENT FUNCTIONALIZATION OF GRAPHENE OXIDE WITH PORPHYRINOIDS

3.3.1. Recent Studies and Applications

Based on the above, it is not surprising that several researches have focused on the bonding (mostly noncovalent) between porphyrinoids and graphene oxide, with positive results. [13-16] Most of them focus on porphyrins as target species for functionalization, while porphyrazines have been much less studied in this area.

The utility of GO/porphyrin hybrids as sensors for specific cancer biomarkers, particularly in detecting circulating tumor cells (CTCs), has been demonstrated.[17] These hybrids play a crucial role in enhancing diagnostic accuracy and improving current methodologies for early cancer diagnosis. Furthermore, they can serve as *turn off-on* sensors, capable of detecting and stabilizing G-quadruplex DNA structures, potentially inhibiting the role of telomerase in cancer cells.

Moreover, the combination of porphyrins and GO in hybrid materials has resulted in various biomedical applications, particularly as photosensitizers in photodynamic therapy (PDT) and photothermal therapy (PTT). For example, noncovalent hybrids between GO and PS molecules such as chloro e6,[18] as well as covalent hybrids with hematoporphyrin,[19] and other porphyrin and phthalocyanine derivatives, have shown enhanced efficiencies in $^1O_2$ production. Currently, there are no studies in the literature reporting the coupling between graphene and porphyrazine derivatives for applications in cancer therapies, and GO functionalization itself with these molecules has been reported only in few cases.[20]

3.3.2. Phototherapies

Photodynamic therapy (PDT) is one of the currently clinically approved strategies for cancer treatment. The main advantage of this kind of therapy provides is its low invasiveness and high selective cytotoxic activity towards cancerous cells.[21] It consists of administering, systemically or

topically, a photosensitizer (which accumulates in the targeted tumor tissue) and irradiating it with light at a specific wavelength inside the so-called phototherapeutic window (600-800 nm region) in the presence of oxygen.[22] This results in the generation of reactive oxygen species (ROS), including singlet oxygen ($^1O_2$). This species is a potent oxidant and attacks cancer cells, inducing their death by apoptosis or necrosis.

Another particularly promising phototherapy is Photothermal Therapy (PTT), in which nonradiative decay of the substance converts electron excitation energy into heat, which is responsible for the cytotoxic effect on diseased cells.[23]

All the major processes involved in PDT-PTT therapies are summarized in the Jablonski Diagram shown in Figure 7.

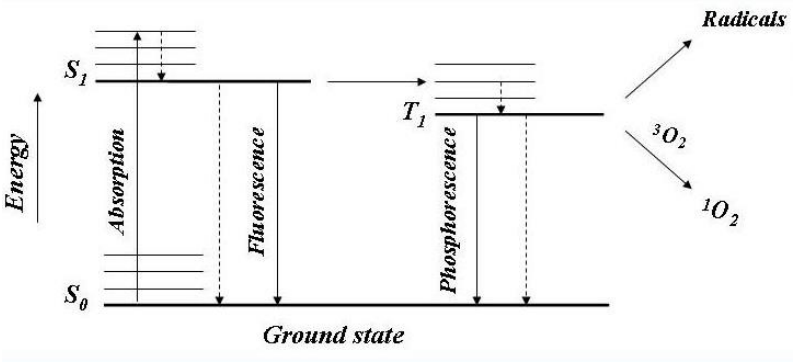

Figure 7. Jablonski Diagram showing the physical and chemical processes involved in PDT and PTT.

Tetrapyrrolic macrocycles, such as porphyrins, phthalocyanines, and porphyrazines, are the most studied categories of compounds in phototherapies,[24,25] but their low solubility in the aqueous medium requires the use of appropriate carrier agents that make their delivery possible.

In recent years, GO-porphyrinoide hybrid materials are receiving particular attention as PDT and PTT agents, stimulating the research toward the preparation of systems with a combined anticancer action.

4. OBJECTIVES

As illustrated in the Introduction, functionalization of graphene oxide with porphyrazine macrocycles can be exploited to obtain a hybrid nanostructure with specific physico-chemical features, in which the two units, GO and macrocycle contribute individually but synergistically to determine the features and the potential of the final novel material.

Thus, the primary objective of this research is to achieve a non-covalent functionalization of GO with porphyrazine molecules, in order to obtain a stable hybrid product with a fair solubility in water. Noticeably, the present work represents one of the first attempts of functionalization of GO with porphyrazine macrocycles.

The selected complex is $[(PtCl_2)_4LZn]$, previously described by Donzello et al., having a chemical structure reported in Figure 6 with M = Zn^{II}. The complex has an exocyclic coordination of four cisplatin-like $PtCl_2$ units in a novel structural arrangement. Moreover, the high value of $^1O_2$ quantum yield obtained in DMF, configures it as a potent photosensitizer for PDT applications with perspectives also in bimodal therapies.

The preparation of the macrocycle-GO hybrid (named Pz@GO) will be optimized step-by-step and, in parallel, the characterization of the hybrid will be carried out by conventional techniques, including UV-Visible and IR spectroscopy, fluorescence measurements, and Raman spectroscopy. These techniques will provide us insights on the structural and electronic properties of the novel material, in order to evaluate potential applicative aspects.

Finally, the non-covalent anchoring of $[(PtCl_2)_4LZn]$ to GO represents the first strategy to vehiculate this hydrophobic photosensitizer in the aqueous medium. Therefore, a key aspect of interest will be to investigate on the efficiency of the novel material Pz@GO in the photoproduction of $^1O_2$ in aqueous solution, for possible application in PDT.

5. EXPERIMENTAL SECTION

5.1. MATERIALS AND METHODS

5.1.1. Solvents and Reagents

MilliQ water was used as solvent. Dimethylformamide (DMF, RPE C. Erba) was used as purchased. 9,10-anthracenediyl-bis(methylene)malonic acid was a commercial product from Sigma Aldrich and was used without further purification. $PcAlS_{mix}$ was previously prepared locally and used as reference standard in photoactivity measurements. It is formulated as described in section 5.3.5.

5.1.2. Graphene Oxide

The batch of graphene oxide (GO) used for the following experiments was synthesized by the group of Prof. Marrani at the Department of Chemistry of Sapienza - University of Rome from graphite by reaction with potassium permanganate, sodium nitrate and sulphuric acid (Hummers' oxidation method). It was spectroscopically characterized in the present work.

IR (cm^{-1}, KBr): 3380(broad), 1723(sh), 1614(vs), 1376(s), 1078(w), 1039(m), 873(m), 236(w).

UV-Vis, λ (nm) in H_2O: 310 (sh), 230.

Raman (cm^{-1}): 1362(vs), 1600(vs), 2756(s), 2945(vs).

5.1.3. $[(PtCl_2)_4LZn]$

The general structure of the porphyrazine under investigation, denoted as $[(PtCl_2)_4LZn]$, was described in the Introduction. The complex was prepared by the group of Prof. Viola at the Department of Chemistry at Sapienza - University of Rome, as previously reported. The physico-chemical characterization of the sample used for the GO functionalization has been completed during this thesis work and the spectroscopic data obtained has been compared with those reported in the literature.

IR (cm^{-1}, KBr): 3500(broad), 1593(m), 1477(s), 1447(m), 1353(s), 1236(vs), 1188(s), 1116(s), 1101(s), 1013(w), 951(s), 850(w), 768(m), 705(vs), 651(m), 557(w), 491(w), 434(w), 341(w) (ν Pt-Cl).

UV-Vis, λ (nm) (log ε in DMF/HCl): 662 (5.34), 631 (sh) (4.45), 600 (4.44), 395 (4.90).

Elemental analysis: Calcd for $[(PtCl_2)_4LZn]\cdot 15H_2O$, $C_{64}H_{62}Cl_8N_{24}O_{15}Pt_4Zn$: C, 30.30; H, 2.46; N, 13.25; Pt, 30.76. Found C, 31.01; H, 2.03; N, 12.32; Pt, 30.94%.

5.2. SYNTHESIS OF THE HYBRID MATERIAL PZ@GO (BATCHES PP01, PP01_2)

1.75 mg of the porphyrazine $[(PtCl_2)_4LZn]$ was dispersed in 5 mL of DMF ($c = 1{,}38\cdot 10^{-4}$ M) and 10.0 mg of graphene oxide (previously dialysed in water for 72 h) was dispersed in 3 mL of MilliQ water. Both solutions were irradiated by an ultrasonic bath until the dispersion was optimal. Then, the GO solution was added dropwise into the porphyrazine solution under vigorous stirring. The final dispersion was then left under stirring for 20 h at room temperature. The dispersion was centrifuged for 30 min at 5000 rpm, the supernatant was separated from the precipitate and the resulting solid was washed two times with MilliQ water (5 mL). Because of the very low concentration of product in the supernatant, the focus remained only on the precipitate. In order to further remove the DMF, the precipitate was dispersed in 10 mL of MilliQ water and the dispersion was dialysed using a membrane with a 12-14 kDa molecular weight cut-off. The membrane was first activated by placing it in a beaker with water for 30 minutes. The dispersion was then added inside the membrane and it was placed in MilliQ water for 72 h. During this period, MilliQ water was changed three times a day. Next, the sample was properly pre-frozen by placing it in a freezer for 24 hours or using liquid N_2 for a few minutes, and then it was successfully freeze-dried using a freeze-dryer for 24 hours. Finally, the dry solid was recovered, weighed and characterized. For batch PP01, an amount of 3.3 mg was obtained. The described procedure was repeated once more and batch PP01_2 was prepared (3.1 mg obtained).

Save for the freeze-drying step, this procedure was repeated to better investigate on the effect of the complete solvent removal from the sample (Batch PP01_3).

IR (cm^{-1}, KBr): 3346(broad), 2904(vw), 2319(w), 1705(vw), 1592(vs), 1477(w), 1352(s), 1236(s), 1187(m), 1100(m), 1057(m), 950(m), 753(vw), 704(s), 649(w), 554(vw), 430(w), 278(m), 264(m), 239(m)

UV-Vis, λ (nm): 668(s), 604(w), 233(vs)

Raman Bands (cm^{-1}): 2953(m), 2816(w), 1606(vs), 1353(vs), 521(w)

5.3. PHYSICAL MEASUREMENTS

The different types of physical techniques used in the present work are summarized here below.

5.3.1. UV-Visible Spectroscopy

For UV-Visible spectroscopy, a spatula tip of the sample was dispersed in MilliQ water and a few mL of the dispersion was added to a 1-cm or 1-mm quartz cuvette. The cuvette was placed in the Varian Cary 50 spectrometer and an UV-Visible spectrum was recorded. For the baseline, the same cuvette was previously filled with the solvent only, in order to neglect absorptions not caused by the product itself. UV-visible spectra were acquired in DMF and in MilliQ water.

5.3.2. Infrared (IR) Spectroscopy

A spatula tip of the sample was well mixed in a mortar into 100 mg of anhydrous KBr (previously dried in the heater at 120 °C for 24 h). The powder was put into a pellet-forming die and pressed with a force of approximately 6 tons using a hydraulic press under vacuum to form a thin transparent pellet. The pellet was then analysed with a Varian 660 FT-IR spectrometer in the range 4000-250 cm^{-1}. As a baseline, a pellet with KBr only is assembled.

5.3.3. Fluorescence Spectroscopy

Steady-state fluorescence spectra were recorded with a Fluorescence Spectrophotometer (Fluoromax 2 - HORIBA Jobin Yvon Ltd) using a 1 mm-quartz SUPRASIL cuvette.

In all experiments, the absorbances of the solution were around 0.1 at and above the excitation wavelength. For the emission and excitation spectra, emission filters were used to prevent the spectra from showing second-order excitation light.

5.3.4. Raman Spectra

A spatula tip of the sample was dissolved in water. Next, a droplet of the solution was placed on a silicon wafer. This wafer was then analyzed with a Renishaw InVia micro-Raman spectrometer, 20x objective, equipped with a 514-nm laser line.

5.3.5. Singlet oxygen photoproduction in water

Tests on the efficacy of the hybrid material GO@Pz to generate $^1O_2$ were performed in aqueous solution using $PcAlS_{mix}$ as reference standard (Pc: phthalocyaninato dianion, $[C_{32}H_{16}N_8]^{=}$).

$PcAlS_{mix}$ (Photosens®) is a mixture of compounds with different sulfonation degree and different isomers having formula $PcAlOH(SO_3Na)_n$ with <n> ~ 3. A sample of $PcAlS_{mix}$ had been previously prepared and characterized in the laboratory of Prof. Viola and it was used for these measurements.

The method used to evaluate the efficacy of the material in the production of $^1O_2$ in water analyzes the decomposition of the $^1O_2$ scavenger ADMA (tetrasodium-9,10-anthracenediyl-bis(methylene)malonate), obtained from the corresponding acid salted with NaOH up to pH ~ 7. A profile of the procedure used for the sample and the reference is as follows.[26]

A water solution (2.00 mL) of the investigated material and the scavenger ADMA ($c \sim 5 \cdot 10^{-5}$ M) was irradiated in a 1.00 cm-quartz cell by a laser source (Premier LC Lasers/HG Lens, Global Laser) in the region of the Q band (λ_{irr} = 660 nm). Illumination was directed normally both to the surface of the solution and to the spectrophotometric radiation. During the experiment, continuous magnetic stirring ensured homogeneity of the solution while a circulating water system kept the temperature constant at 25 °C. The power of irradiation (*W*), accurately measured by a radiometer (ILT 1400A/SEL100/F/QNDS2, International Light Technologies), was fixed at ca. 21 mW..

The trap's absorption at 380 nm was monitored as a function of the time, and sensitizer stability was also checked under irradiation. It can be demonstrated that, because of the fast decay of $^1O_2$ in aqueous solution, the photo-oxidation of the scavenger ADMA, under the experimental conditions described above, follows a first-order kinetic equation. The relative photosensitizing activity of the material in the production of singlet oxygen, $^1O_2$, with respect to the reference $PcAlS_{mix}$ can be evaluated on the basis of the following equation:

$$Relative\ photosensi\ tizing\ activity = \frac{k_I W_{abs}^R}{k_I^R W_{abs}}$$

where k_I and k_I^R are the ADMA bleaching first-order rate constants of the sample and the reference $PcAlS_{mix}$, respectively; W_{abs} and W_{abs}^R are the rate of light absorption by the examined cation and the reference, respectively, calculated considering an optical path length of 2.1 cm (total volume of solution and magnet in the cuvette = 2.1 mL); $W_{abs} = W(1\text{-}10^{-2.1A})$.

6. RESULTS AND DISCUSSION

In this section, all spectroscopic characterizations performed on the materials (starting and novel) will be discussed and the results compared. In the following discussion, the complex $[(PtCl_2)_4LZn]$ will be referred to as Pz, the starting graphene oxide as GO, and the hybrid material as Pz@GO.

6.1. PREPARATIVE ASPECTS AND UV-VISIBLE SPECTRA

6.1.1. Solvents for the synthesis of Pz@GO

In the Pz@GO synthesis procedure, Pz was dissolved (partially dispersed) in N,N-dimethylformamide (DMF) and this mixture was then added to an aqueous dispersion of GO. The choice of dissolving porphyrazine in DMF instead of adding it directly to the aqueous medium is a critical consideration that deserves further investigation. DMF, as a low-donor polar solvent, offers distinct advantages for solubilizing porphyrazine, preventing aggregate formation, and promoting optimal interactions with graphene oxide. By effectively solubilizing Pz in its monomeric form, DMF ensures individual separation of porphyrazine molecules, thus facilitating their availability for interactions with graphene oxide.

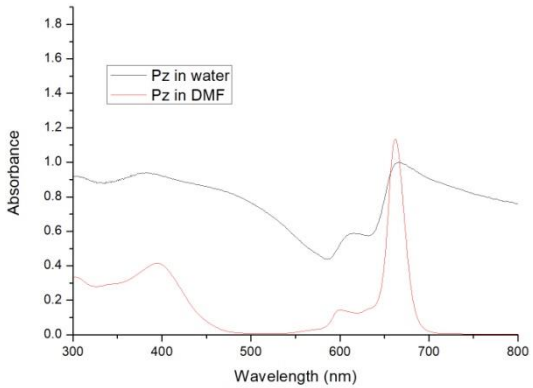

Figure 8. UV-Visible Absorption Spectra of $[(PtCl_2)_4LZn]$ in water and in DMF.

Figure 8 shows the comparison of the UV-visible spectra of Pz obtained in DMF and in water. The spectrum in DMF is typical of a porphyrazine macrocycle present in solution in its monomeric

form and characterizes Pz up to the saturation limit, with a narrow Q band in the 600-700 nm range (λmax = 662 nm). In contrast, the H_2O dispersion of Pz shows only a broad absorption in this region, with a scarcely detectable Q- band maximum at 667 nm, indicative of molecular aggregation due to interactions π-π. In addition, all the spectrum displays consistent scattering, which can be attributed to the presence of the porphyrazine aggregates.

This different behaviour in the solvents is visually apparent, as the water dilution displays irregular dispersion in suspension, while porphyrazine in DMF appears homogeneously solubilized. Thus, both spectroscopic and visual observations support the conclusion that DMF promotes effective solubilisation of porphyrazine, preventing the formation of aggregates.

On the other hand, the insolubility of Pz in the aqueous medium encourages the search for appropriate carrier agents that make its administration possible.

6.1.2. GO in H_2O

In Figure 9 the UV-visible spectrum of GO in H_2O in the range 800 - 200 nm is presented. It shows two characteristic peaks: a shoulder at about 310 nm due to π-π* transitions of C=O carbonyls and a peak at about 230 nm due to π-π* transitions of C=C bonds. These features are in line with values reported in the literature.

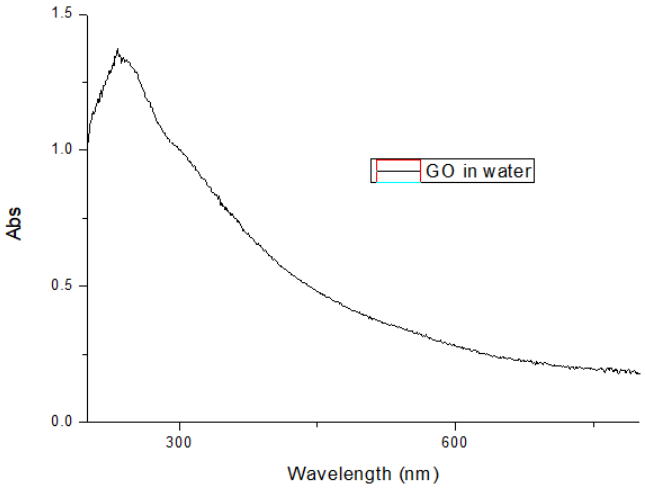

Figure 9. UV-Visible Absorption Spectrum of GO in water.

The UV-visible GO spectrum in water provided a useful starting point for studying the effect of functionalization of the material with the porphyrazine complex.

6.1.3. Dialysis Effect

The properties of the obtained hybrid material in water have been one of the major interests for our study. Therefore, despite the usefulness of DMF during the synthesis, its subsequent removal becomes necessary. This is accomplished through a two-step process. Firstly, centrifugation is performed to separate the precipitate from the supernatant, which contains the majority of the DMF. The resulting precipitate is then subjected to thorough washing with MilliQ water. However, this process alone proves insufficient, as evidenced by the spectrum of the obtained material shown in Figure 10 (PP01 Precipitate). Consequently, dialysis is deemed necessary to ensure the complete removal of DMF.

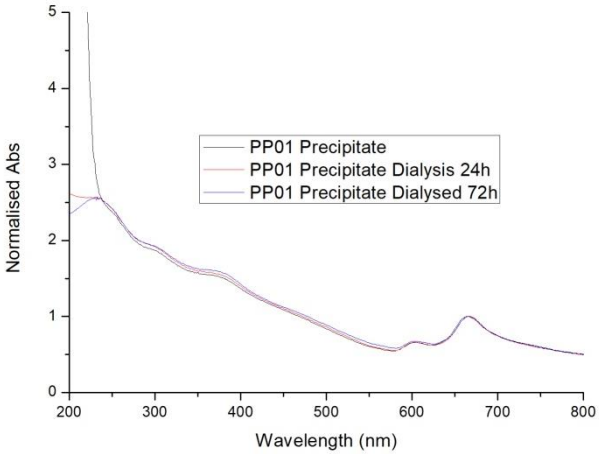

Figure 10. UV-Visible Absorption Spectra of Pz@GO before dialysis (PP01 Precipitate), after 24h of dialysis (PP01 Precipitate Dialysis 24h) and after 72h of dialysis (PP01 Precipitate Dialysed 72h).

The spectra reported in Figure 10 clearly indicate that prior to dialysis, the hybrid species retained a significant amount of DMF, as evidenced by the pronounced absorption in the 250 nm region in which the solvent absorbs. Furthermore, the effectiveness of dialysis is evident, as within the initial 24-hour period, there is a substantial reduction in absorption within that range. Impressively, this trend continues even after 72 hours of dialysis, with a slight further decrease in absorption observed. These results suggest that most of the DMF was successfully removed

through the dialysis process, resulting in almost complete subtraction of its presence within the hybrid species.

6.2. SPECTROSCOPIC CHARACTERIZATION OF THE HYBRID MATERIAL PZ@GO

6.2.1. UV-Visible Spectra Analysis

To evaluate the effectiveness of the functionalization process, the UV-Visible absorption spectrum of the hybrid material after 72 hours of dialysis is compared with the UV-Visible absorption spectra of graphene oxide and porphyrazine individually in water. This comparative analysis allows us to assess the extent of successful functionalization and to examine any characteristic shifts or new absorption features that may indicate the formation of the desired hybrid structure. The juxtaposing of these spectra (Figure 11) allows us to gain insights into the spectral signatures and confirm the presence of the desired functionalization in the hybrid material.

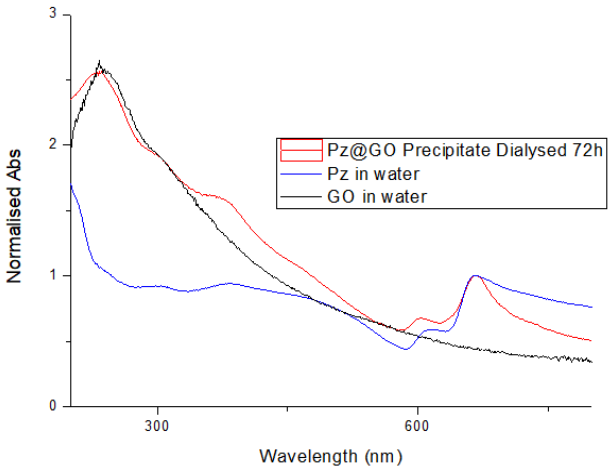

Figure 11. UV-Visible Absorption Spectra of Pz@GO in water after 72h of dialysis, Pz in water and GO in water.

For better comparison, the spectra have been normalised at 300 nm (those of graphene oxide and the hybrid material) and at 667 nm (those of porphyrazine and the hybrid material).

The spectra provide clear evidence of the obtained functionalization of the GO with the porphyrazine macrocycle, the hybrid material exhibiting characteristic bands of both.

As described above, in aqueous medium the graphene oxide (GO) shows significant absorption in the 200-400 nm range, while the porphyrazine (Pz) spectrum exhibits a very broad Q band with a maximum at 667 nm and a less intense vibrational component with λ_{max} = 615 nm. Less defined but present are the absorption in the Soret region, in the 200-400 nm range which overlap with the GO spectrum. Remarkably, the spectrum of the hybrid system Pz@GO shows both the absorption in the 200-400 nm range (with the visible contribute from graphene oxide and porphyrazine) and a well-defined band with λ_{max} = 667 nm clearly due to the porphyrazine. Notably, the vibrational component is also clearly identifiable in the spectrum of the hybrid material, although slightly shifted to lower wavelengths (604 nm).

Furthermore, these spectra provide valuable insights into the effect of non-covalent coupling with GO on the water solubility of the Pz macrocycle, an aspect of great interest in this work. Although the hybrid material is still dispersed in water, there is a significant decrease in the absorption coefficient in the 700-800 nm range compared to that of pure porphyrazine. The Q band is more defined and this effect clearly indicates that the non-covalent interaction of Pz with GO reduces the molecular aggregation between porphyrazine macrocycles, with an enhancement of the porphyrazine present in the aqueous medium in its monomeric, thus better solubilized, form. This aspect is the quantitative evaluation of the higher solubility of Pz in H_2O within the Pz@GO hybrid will be the subject of further investigation. The stability of the hybrid material in water through time is very straightforward; as time goes by, the material slowly precipitates decreasing the concentration in solution as well as the aggregation. UV-Visible evidence of this fact can be found in Appendix 1.

6.2.1.1. Dilution Experiment of Pz@GO in water

In order to obtain more information about the nature and stability of the hybrid system, and also about the presence of equilibria in solution involving Pz in different forms (Pz@GO or molecular aggregates or free monomers), a dilution experiment of a Pz@GO solution in water has been carried out to check whether or not the Lambert-Beer Law was obeyed. Starting from a Pz@GO solution in water, four successive 1:1 dilutions were performed. The results are shown in Figure 12.

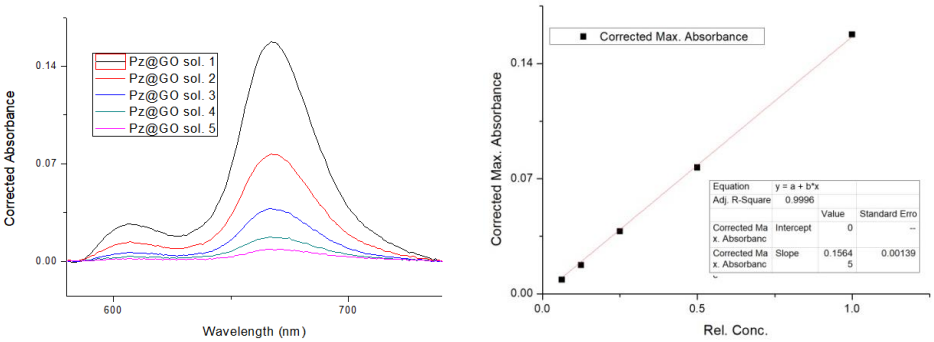

Figure 12. Left (A): UV-Visible Absorption Spectra of Pz@GO at different concentrations (sol. 1-5 in decreasing concentration). Right (B): The maximum absorbance of each solution vs its relative concentration and its linear fit.

Figure 12A shows the spectra obtained and elaborated within the spectral window including the porphyrazine's Q-band. To account for scattering caused by GO dispersion, the pristine spectra have been appropriately baselined using the Morton-Stubbs 3-point correction.[27] In Figure 12B, the maximum absorbance of the Q-band is plotted for each solution relative to its concentration. The most concentrated solution is assigned a concentration value of 1, while the remaining concentrations are assigned proportionally. Notably, the data exhibits an exceptional level of linearity (R^2: 0.9996), firmly adhering to the Lambert-Beer Law. Based on this compelling evidence, it can be confidently concluded that the non-covalent functionalization has been highly likely successful, as only one Pz species is present in the water solution.

6.2.1.2. The effect of Freeze-Drying

Once sufficient evidence has been gathered to support the successful synthesis of the hybrid material, it becomes advantageous to proceed with freeze-drying the suspension to obtain a solid form. The advantages of having the material in a solid state are twofold: firstly, it allows for determination of the reaction yield, and secondly, it enables further characterization of the material using, for example, IR spectroscopy.

However, an unexpected event occurred when the material was freeze-dried. After redissolving the solid sample in MilliQ water, a very differently shaped UV-Visible spectrum was observed. Scattering phenomena clearly prevailed over distinguishable bands and the spectrum was essentially flat with hardly perceptible small absorptions (Figure 13).

The second derivative spectra calculated in the Q-band region are shown in the inset of Figure 13 and aid in the interpretation of the UV-visible spectrum. It is interesting to note that, even if the Pz seems to be absent, the absorption maxima markedly present in the spectrum of Pz@GO in H_2O before freeze-drying are still appreciable in the spectrum of the freeze-dried material (good correspondence of the minima of the second derivative curves) and in the latter one a small additional absorption with maximum at about 730 nm is present.

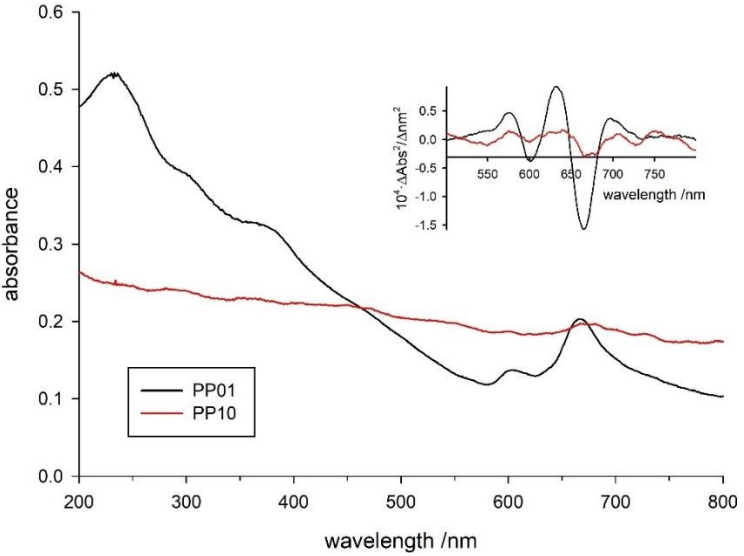

Figure 13. UV-Visible Absorption Spectra of Pz@GO in water before (black line) and after (red line) freeze drying. The inset shows the 2nd derivative of both spectra with respect to the wavelength.

The exact cause of this phenomenon remains unclear. One hypothesis is that the removal of water and any residual DMF during the freeze-drying process brings GO and Pz system even closer together, allowing the formation of stable aggregates based on π-π interactions and/or interactions between GO oxygen-based functional groups and the multiple heteroatoms present in the porphyrazine macrocycle. This increased proximity could promote a more efficient Pz-GO coupling that could not be easily reversed upon redissolution, and a marked scattering effect in the reconstituted dispersion is observed as if it were in a semi-solid state. The interaction could be able to modify the electronic structure of the single units, leading to important changes in the absorption spectrum (loss of resolution and red shift of the absorption bands). These features

seem to resemble those found for other aromatic macrocycles, for which the interaction with the GO induced distortions in the rigid planar structure of the macrocycle.[28] This experimental evidence deserves further investigation that goes beyond the scope of this report.

6.2.2. Characterization by Photoluminescence Spectra

As pointed out before, introducing oxygen-containing groups into graphene lattice means that GO nanosheets exhibit many amazing properties, such as excellent water dispersibility, surface modifiability, biological compatibility, and so on. The most notable is that the infinite large sp^2 domain is disrupted after oxidizing, and the bandgap can be opened to transform the non-luminescent graphene into luminescent GO.

The photoluminescence (PL) spectra of GO used to prepare the hybrid Pz@GO are reported in Figure 13. The sample has been excited at different wavelength, corresponding to the absorption main peaks shown by GO. The intensity of the PL spectra reflects the different absorptivity shown by GO at the different wavelengths while the shift in the PL emission bands upon changing the excitation wavelength is a typical behaviour of GO.

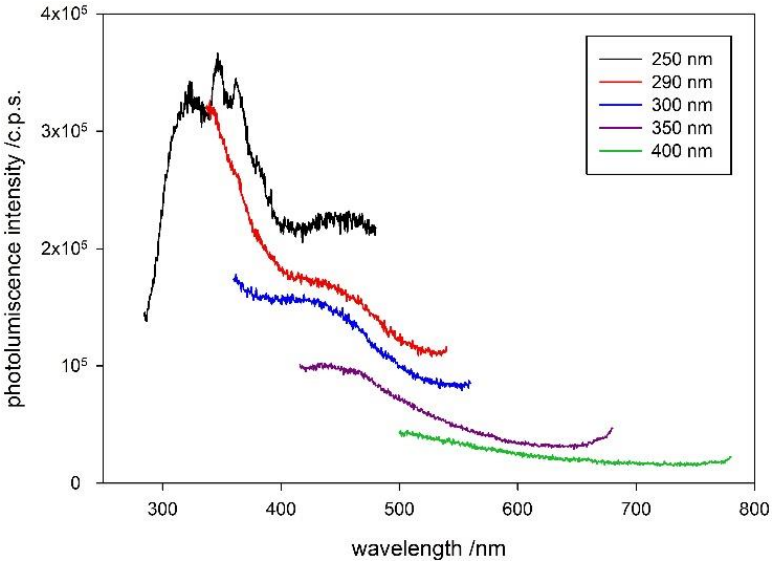

Figure 14. Photoluminescence (PL) spectra of GO in water excited at different wavelength (see legend - slit width: 5/5 nm) at a concentration such as its absorption at 300 nm was 0.1. For the spectrum measured with λ_{exc}= 290 nm, only the region 337-540 nm in order to remove the water Raman scattering band centred at around 322 nm (whose intensity was much higher than the GO luminescence).

A comparison of the PL spectra reported in Figure 13 with those relative to the Pz@GO samples reported in Figures 14 and 15 (before and after the freeze-drying process, respectively) clearly shows that the Pz fluorescence cannot be detected in both samples. This is not surprising since it is well known that even direct conjugation of fluorophores onto GO nanosheets always failed to endow its fluorescent ability because of resonance energy transfer mechanism that result in the complete quenching of the fluorophore.[29]

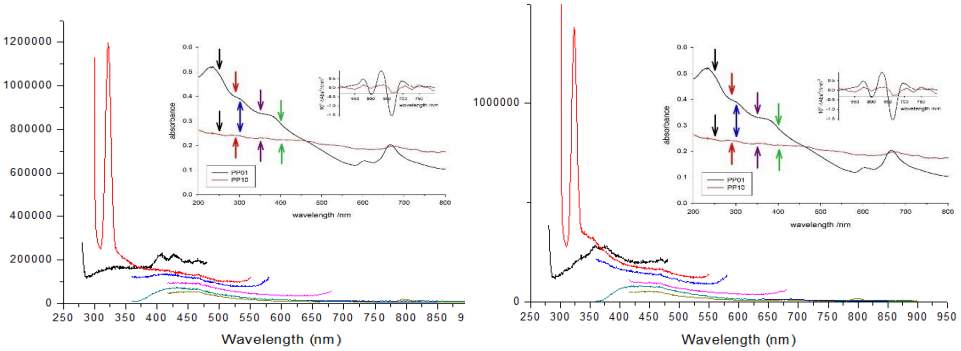

Figure 15. A (Left): Photoluminescence spectra of Pz@GO before the freeze-drying process, in H_2O(colours refer to the excitation wavelengths - see the Inset). Slits: 5/5 nm. B (Right): Photoluminescence spectra of the freeze-dried Pz@GO sample, in H_2O (colours refer to the excitation wavelengths - see the Inset). Slits: 5/5 nm.

From the luminescence point of view, both samples behave similarly; producing spectra barely discernible by those of GO alone at all the excitation wavelengths probed. Not only the Pz fluorescence is quenched by the interaction with GO, but it wasn't possible to detect any energy transfer from GO to Pz that would have been resulted into a Pz fluorescence band falling in the 620-780 nm region.

To check if the interaction with GO somewhat altered the Pz molecule, a known volume of the freeze-dried sample was resuspended in DMF. Fluorescence spectra were then acquired to cover a time span of about two days (Figure 17).

The intensity of the fluorescence spectra increased significantly over time, and after about two days the kinetics of the process of desorption of Pz from GO reached a steady state (inset of Figure 17). This evidence matched with what recorded for the same sample by UV-Vis spectroscopy (Figure 18). Both the fluorescence and the absorption spectra closely resembled those of Pz in DMF, ruling thus out any irreversible alteration of the macrocycle.

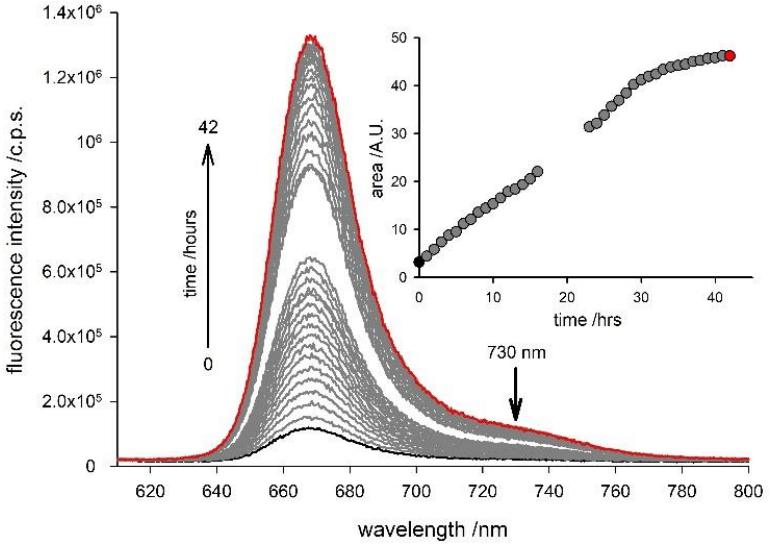

Figure 17. Emission spectra of the freeze-dried sample resuspended in DMF over time (black line: first spectrum; red line: last spectrum). The arrows at 730 nm indicates the wavelength where the excitation spectra of Figure 18 have been collected. The inset shows the area of the emission peak as a function of time (same colours as in the main graph). λ_{exc}= 600 nm; slits: 2.5/2.5 nm; T= 25 °C.

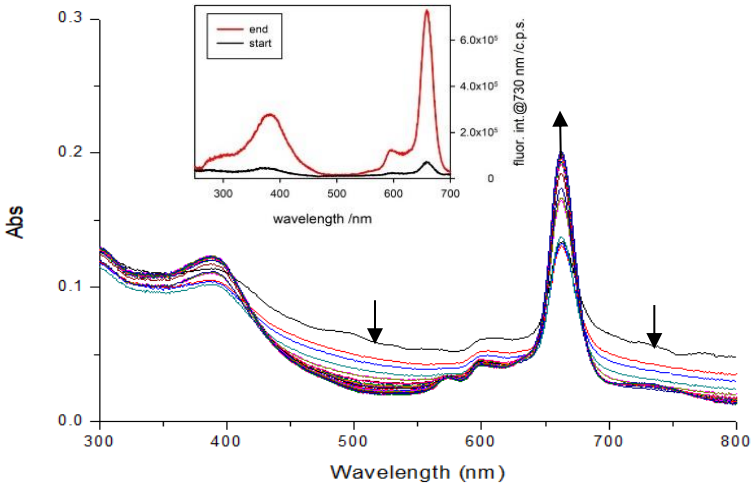

Figure 18. Absorption spectra of the freeze-dried Pz@GO sample in DMF with time. The inset shows the excitation spectra (λ_{em}= 730 nm; slits: 2.5/2.5 nm; 660 nm high-pass filter; T= 25 °C) recorded at the beginning and at the end of the fluorescence experiment of Figure 17.

6.2.3. IR AND RAMAN CHARACTERIZATION

6.2.3.1. FT-IR spectra

As previously stated, the freeze-drying process of the aqueous samples resulted in a solid material suitable for characterization by FT-IR spectroscopy in KBr pellets. Figure 19 shows the IR spectra obtained for GO, Pz and the hybrid material Pz@GO.

The FT-IR spectrum of GO (blue line) shows the C=O feature at 1723 cm^{-1} belonging to aldehydes, ketones and carboxyl groups and another one at 1614 cm^{-1} assigned to the bending modes of adsorbed water molecules. The last two signals in the range of 1000-1100 cm^{-1} are attributed to the C–O/C-O-C stretching modes.

The FT-IR spectrum of porphyrazine (red line) matchs very well with that reported in the literature.[11] A noteworthy feature is a low intensity absorption at 341 cm^{-1} which is assigned as the stretching ν(Pt−Cl) mode and is indicative of the presence of the peripheral $PtCl_2$ units. As to the macrocyclic system, the vibrations of the central porphyrazine core are strongly coupled with those of annulated pyrazine heterocycles. As a result, the present pyrazinoporphyrazine macrocycle have a unique IR spectroscopic pattern which is quite different from that of the phthalocyanine analogue.

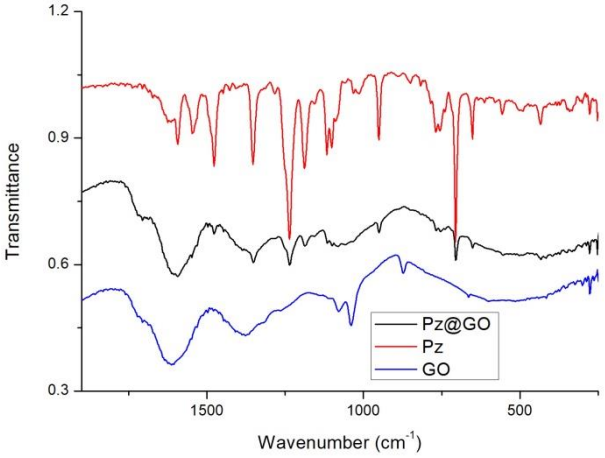

Figure 19. FT-IR Spectra of GO (blue line), Pz (red line) and Pz@GO (after the free-drying process, black line).

Some pertinent assignments can be suggested on the basis of literature data on analogue compounds. The skeletal stretching vibrations of the pyrazinoporphyrazine ring − including those of pyrrole rings, stretching ν(CN) and ν(CC) of annulated rings and stretching vibrations involving the meso-N atom bridge, typically at 1500-1550 cm^{-1} − give medium and intense absorptions in the range 1100–1600 cm^{-1}. The in-plane deformations of the pyrrole rings and of annulated pyrazine heterocycles are in the range 900–1100 cm^{-1} while the corrisponding out-of-plane deformations appear in the range 600-800 cm^{-1}. Pyridine rings contribute with a ring vibration at ca. 1200 cm^{-1} and an absorption in the range 900-1000 cm^{-1} associated to CH wadding mode.

Moving to the IR spectrum of Pz@GO, comparison with GO and Pz spectra provides information information on the composition of the hybrid material. Noteworthy, the most intense bands of Pz are present in the spectrum of the hybrid Pz@GO (black line), confirming that non-covalent conjugation has occurred.

It is important to note that the ν(Pt−Cl) stretching at 341 cm^{-1} doesn't seem to be present in the spectrum of Pz@GO. The absorption, very weak, could be present but not detectable; on the contrary, this feature could be indicative of a partial or total hydrolysis of the Pt−Cl bond in the aqueous medium. Preliminar experiments have been conducted to explore this aspect, but further investigation is required.

6.2.3.2 Raman spectra

Figure 20 shows the Raman characterization performed on Pz and Pz@GO (the freeze-drying sample). The Raman spectrum of Pz (blue line) had not been acquired previously. It displays plenty of narrow peaks typical of molecular species. In particular, the most prominent ones localized in the range between 1400-1600 cm^{-1} and ascribable to C=N and C=C vibrational modes of aromatic systems, are also observed in the non-covalent conjugate (black line).

Besides, its spectrum shows the typical prominent D and G bands of GO centered at 1362 cm^{-1} and 1600 cm^{-1} relative to the breathing mode of the carbon rings near the structural defects (D band) and C=C stretching vibrations (G band), respectively. Moreover, the second-order bands 2D and D+G localized in the range between 2400-3200 cm^{-1} are also observed.

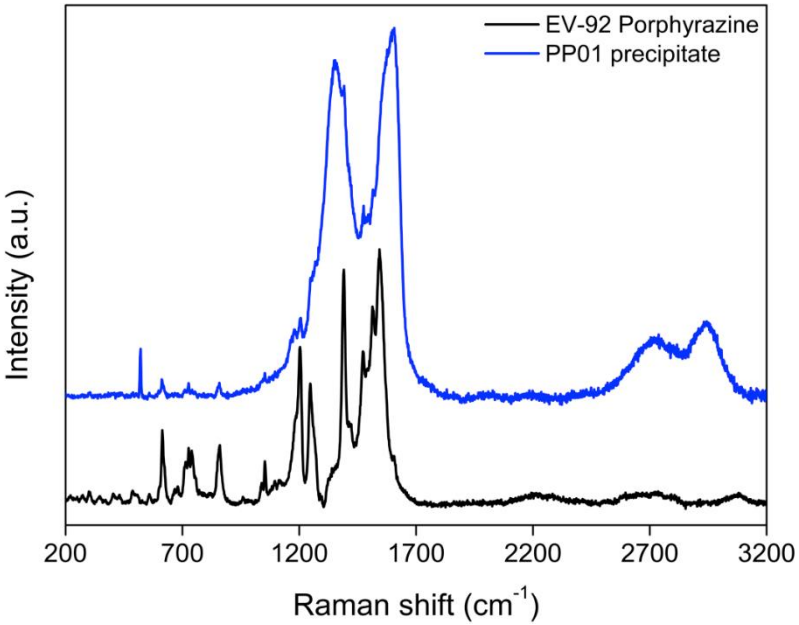

Figure 20. Raman Spectra of Pz (black line) and Pz@GO (after the free-drying process, blue line).

6.3. SINGLET OXYGEN PHOTOPRODUCTION IN WATER SOLUTION

The non-covalent functionalization of GO with Pz represents the first strategy to transport in aqueous medium this hydrophobic complex, which has potentialities to act as photosensitizer in Photodynamic Therapy and in multimodal therapies. Therefore, the efficiency of the novel synthesized hybrid material Pz@GO in the production of singlet oxygen ($^1O_2$) has been tested and a measurement of singlet oxygen quantum yield (Φ_Δ) in H_2O has been planned.

The absolute singlet oxygen quantum yield of Pz in DMF was previously measured[11] and a significant value was obtained (Φ_Δ = 0.52). On the contrary, the quantification of $^1O_2$, generated upon irradiation of a sensitizer in aqueous solution, is not easy to achieve. Indeed, owing to the high efficacy of the quenching of $^1O_2$ by water, the lifetime of $^1O_2$ in this medium is 1-2 orders of magnitude shorter than in organic solvents,[30] i.e. τ_{H2O} = 3 μs; τ_{DMF} = 10 μs. Therefore, the *absolute* determination of the $^1O_2$ quantum yield (Φ_Δ) in water cannot be performed by indirect chemical methods, involving the trapping of $^1O_2$ by a chemical scavenger. For this reason, we decided to perform the photochemical studies in aqueous solution by following a comparative procedure, as reported in the literature.[26,30] As described in the Experimental Section, ADMA (tetrasodium-9,10-

anthracenediyl-bis(methylene)malonate), obtained from the corresponding acid (Figure 21) salted with NaOH up to pH ~ 7, is a water soluble, highly reactive and specific chemical scavenger for $^1O_2$. It was employed for this measurement and the kinetic analysis of its photooxidation reaction due to $^1O_2$ was carried out.

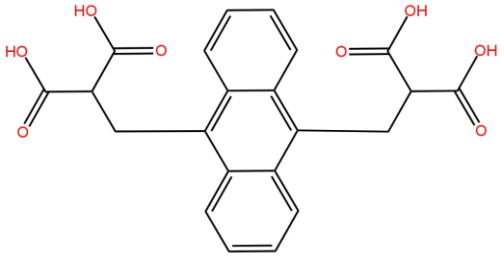

Figure 21. 9,10-Anthracenediyl-bis(methylene)dimalonic acid.

The efficacy of the sensitizer in the production of $^1O_2$ is evaluated by coupling two experiments in one measurement under identical experimental conditions, one for the sensitizer under investigation (Pz@GO) and the other one for the reference standard.

The reference standard used is a mixture of aluminum phtalocyanines with different sulfonation degree and different isomers ($PcAlS_{mix}$ = $PcAlOH(SO_3Na)_n$ with <n>≈ 3) which is a well-known $^1O_2$ sensitizer (Photosens®) that has been widely used for comparison purposes in singlet oxygen quantum yield measurements in H_2O on phthalocyanine or porphyrazine macrocycles.[26] $PcAlS_{mix}$ exhibits monomeric behavior in H_2O showing a spectrum characterized by a narrow Q band at 678 nm (Figure 22). The photosensitizing efficacy in $^1O_2$ production of Pz@GO has been evaluated as "*relative photoactivity*" compared to that shown by the reference standard $PcAlS_{mix}$ under strictly identical experimental conditions.

The results of an experiment performed on Pz@GO are exemplified in Figure 23. It is important to note that the sample used for the photosensitization test was the one obtained before the freeze-drying process, with Q-band absorption clearly detectable. The absorption of light by the sensitizer is in fact the necessary condition for the energy transfer to the triplet oxygen and the generation of singlet oxygen.

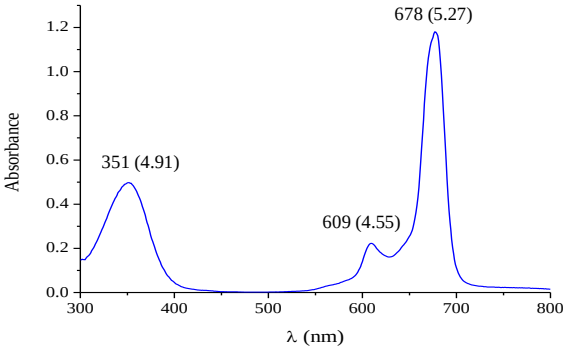

Figure 22. UV-visible spectrum in H_2O of $PcAlS_{mix}$ (c = $6.33 \cdot 10^{-6}$ M); (logε) of absorption maxima are reported on the spectrum.

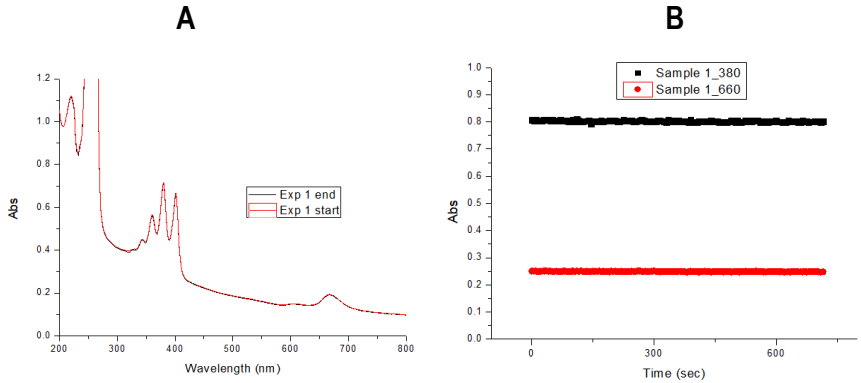

Figure 23. A) UV-visible spectra of Pz@GO and ADMA in H_2O before (red line) and after (black line) laser irradiation (λ_{irr} = 660 nm); B) Absorbance values indicating any ADMA photo-oxidation (black plot) and the stability of the sensitizer Q-band maximum (red dots) during irradiation.

Figure 23-A shows the initial UV-visible spectrum of the solution containing Pz@GO (red line, Q band at 667 nm) and the peaks of ADMA in the region 300-400 nm. The suspension was irradiated with a laser source at 660 nm (W= 21 mW) for more the 10 min and then the UV-vis

spectrum was recorded again. Unfortunately, no ADMA-absorption decay was observed (Figure 23-B), and the final spectrum was superimposed on the starting one. Noticeably, the spectrum of Pz@GO in H_2O remained very stable during irradiation, indicating that the material is not undergoing photobleaching at all.

The experiment was also conducted using the reference $PcAlS_{mix}$ under the same experimental conditions, and the first-order decay of ADMA absorbance at 380 nm was observed (Figure 24). These results seem to indicate that Pz@GO is not a photosensitizing material for $^1O_2$ production.

In order to examine the real experimental conditions under which Pz@GO and the reference PcAlSmix were studied and to better investigate the photosensitizing activity of the hybrid material, we decided to check whether the GO could interfere with the scavenger's reactivity towards singlet oxygen. The scavenger has an anthracene unit with a large π-system and four carboxylate functions: interactions with the GO could make it less reactive towards singlet oxygen, so no decay would be observed.

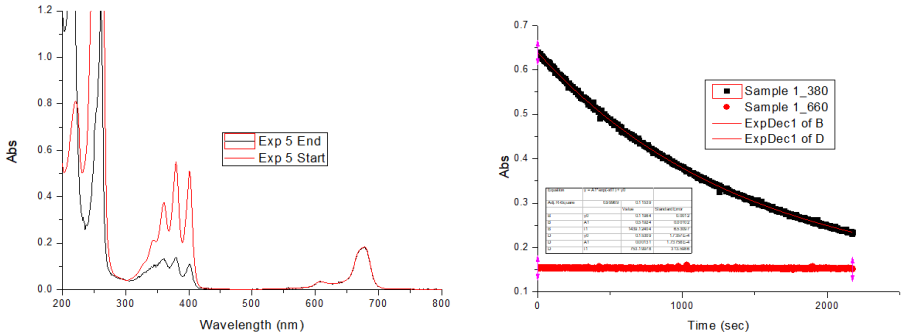

Figure 24. A) UV-visible spectra of $PcAlS_{mix}$ and ADMA in H_2O, before (red line) and after (black line) laser irradiation (λ_{irr} = 660 nm); B) Absorbance values indicating ADMA photo-oxidation (red plot) and sensitizer Q-band maximum (dark dots) during irradiation; the related first-order exponential fit (black line) is also shown.

For this reason, a series of experiments aimed at studying the effect of an increase in GO concentration on the first-order kinetic decay constant of ADMA were planned, having the reference PcAlSmix as the active photosensitizer. In practice, the total volume of the irradiated solution was kept constant (V= 2.0 mL) and the amount of GO was progressively increased by

adding increasing volumes of a stock solution of GO and adjusting those of ADMA and sensitizer accordingly. The data are summarised in Table 1 and the UV-visible spectra are shown in Appendix 2.

Exp.	GO (mL)	Abs $\times 10^{-2}$	W	k $\times 10^{-4}$ (s^{-1})	k' $\times 10^{-5}$ (s^{-1})
1	0	8.78	7.27	6.95	9.56
2	0.200	7.34	6.27	5.53	8.81
3	0.400	5.80	5.14	3.77	7.23
4	0.600	4.50	4.11	3.22	7.83

Table 1. Experimental data on the influence of GO on ADMA reactivity towards $^1O_2$.

In Table 1, *GO* corresponds to the volume of GO stock solution added to the cuvette, *Abs* is the absorbance at 660 nm (irradiation wavelength), i.e. the absorbance baselined by the Morton–Stubbs three-point correction to assess the real absorbance of the $PcAlS_{mix}$, W is the rate of light absorption by $PcAlS_{mix}$ calculated considering an optical path length of 2.1 cm (total volume of solution and magnet in the cuvette = 2.1 mL): $W = W\ (1 - 10^{-2.1Abs})$. The effect of increasing of GO amount on kinetic decay of the scavenger was considered calculating the value of k', i.e. the k normalized to the light absorption by the sensitizer in the different experiments, using the equation: $k' = k / W$. As can be inferred from the obtained value of k', the observed trend is a decrease in the value of k' when the GO concentration increases. These preliminary results (which will need to be reproduced and confirmed) suggest that GO may interfere with the scavenger's reactivity towards singlet oxygen and the measurements of the efficacy of the Pz@GO in the production of $^1O_2$ by this method may not be reliable.

A more suitable method could be the direct detection of the phosphorescence of $^1O_2$ at 1270 nm. This technique is rapid, specific for $^1O_2$ and does not require additional compounds which could perturb the system under study. Further investigation will be conducted in this direction.

7. CONCLUSION

In conclusion, this research successfully achieved the non-covalent functionalization of graphene oxide (GO) sheets with the porphyrazine macrocycle [$(PtCl_2)_4$LZn], an active photosensitizer for $^1O_2$ production, resulting in the synthesis of the stable hybrid material Pz@GO.

Comprehensive characterization techniques, including UV-Visible spectroscopy, infrared spectroscopy (IR), Raman spectroscopy and photoluminescence measurements were employed to evaluate the structural and optical properties of the hybrid material. These analyses confirmed the successful integration of the porphyrazine on GO sheets and provided valuable insights into the features of the hybrid material, in which the two units, GO and Pz, appear to be in close and exceptional proximity.

Furthermore, the hybrid Pz@GO material exhibits improved characteristics of solubility in water compared to pure porphyrazine, favouring the presence of the macrocycle in its monomeric form and contrasting the formation of dimers or other porphyrazine aggregates. This behaviour is of great interest for a potential application of the new material Pz@GO in the field of Photodynamic Therapy and other multimodal therapies. However, the problematic aspect of water solubility needs for further optimization.

Unfortunately, the investigation on the photosensitizing efficiency of the hybrid material in the production of the $^1O_2$ did not provide reliable information, but highlighted the need to select a suitable method to conduct this type of investigation on such hybrid systems.

Finally, all the results obtained in this Thesis Work lay the foundation for future investigations and potential biomedical applications, further advancing the understanding and utilization of porphyrazine-graphene oxide hybrids in various fields, including Photodynamic Therapy.

8. REFERENCES AND NOTES

1. Konios, D.; Stylianakis, M. M.; Stratakis, E.; Kymakis, E. Dispersion Behaviour of Graphene Oxide and Reduced Graphene Oxide. *J Colloid Interface Sci* **2014**, *430*, 108–112. https://doi.org/10.1016/j.jcis.2014.05.033.
2. Georgakilas, V.; Otyepka, M.; Bourlinos, A. B.; Chandra, V.; Kim, N.; Kemp, K. C.; Hobza, P.; Zboril, R.; Kim, K. S. Functionalization of Graphene: Covalent and Non-Covalent Approaches, Derivatives and Applications. *Chem Rev* **2012**, *112* (11), 6156–6214. https://doi.org/10.1021/cr3000412.
3. Jiříčková, A.; Jankovský, O.; Sofer, Z.; Sedmidubský, D. Synthesis and Applications of Graphene Oxide. *Materials* **2022**, *15* (3), 920. https://doi.org/10.3390/ma15030920.
4. Monteiro, A. R.; Neves, M. G. P. M. S.; Trindade, T. Functionalization of Graphene Oxide with Porphyrins: Synthetic Routes and Biological Applications. *Chempluschem* **2020**, *85* (8), 1857–1880. https://doi.org/10.1002/cplu.202000455.
5. Kozlov, A. V.; Stuzhin, P. A. Synthesis, Acid-Base Properties, and Deselenation of 5,6,8,9,11,12-Hexakis(4-Tert-Butylphenyl)[1,2,5]Selenadiazolo[3,4-b]Porphyrazine. *Russian Journal of Organic Chemistry* **2013**, *49* (6), 913–921. https://doi.org/10.1134/S1070428013060195.
6. Fuchter, M. J.; Zhong, C.; Zong, H.; Hoffman, B. M.; Barrett, A. G. M. Porphyrazines: Designer Macrocycles by Peripheral Substituent Change. *Aust J Chem* **2008**, *61* (4), 235. https://doi.org/10.1071/CH07445.
7. Lijewski, S.; Gierszewski, M.; Sobotta, L.; Piskorz, J.; Kordas, P.; Kucinska, M.; Baranowski, D.; Gdaniec, Z.; Murias, M.; Karolczak, J.; Sikorski, M.; Mielcarek, J.; Goslinski, T. Photophysical Properties and Photochemistry of a Sulfanyl Porphyrazine Bearing Isophthaloxybutyl Substituents. *Dyes and Pigments* **2015**, *113*, 702–708. https://doi.org/10.1016/j.dyepig.2014.10.004.
8. Rodríguez-Morgade, M. S.; Stuzhin, P. A. The Chemistry of Porphyrazines: An Overview. *J Porphyr Phthalocyanines* **2004**, *08* (09), 1129–1165. https://doi.org/10.1142/S1088424604000490.
9. Donzello, M. P.; Viola, E.; Ercolani, C.; Fu, Z.; Futur, D.; Kadish, K. M. Tetra-2,3-Pyrazinoporphyrazines with Externally Appended Pyridine Rings. 12. New Heteropentanuclear Complexes Carrying Four Exocyclic Cis-Platin-like Functionalities as Potential Bimodal (PDT/Cis-Platin) Anticancer Agents. *Inorg Chem* **2012**, *51* (22), 12548–12559. https://doi.org/10.1021/ic301989a.
10. Gouterman, M.; Wagnière, G. H.; Snyder, L. C. Spectra of Porphyrins. *J Mol Spectrosc* **1963**, *11* (1–6), 108–127. https://doi.org/10.1016/0022-2852(63)90011-0.
11. Cai, X.; Donzello, M. P.; Viola, E.; Rizzoli, C.; Ercolani, C.; Kadish, K. M. Structural, UV−Visible, and Electrochemical Studies on 2,3-Dicyano-5,6-Di-2-Pyridylpyrazine, [(CN) $_2$ Py $_2$ Pyz], Related Species and Its Complexes [(CN) $_2$ Py $_2$ PyzMCl $_2$] (M = Pt ^{II} , Pd ^{II}). *Inorg Chem* **2009**, *48* (15), 7086–7098. https://doi.org/10.1021/ic8023277.
12. Jamieson, E. R.; Lippard, S. J. Structure, Recognition, and Processing of Cisplatin−DNA Adducts. *Chem Rev* **1999**, *99* (9), 2467–2498. https://doi.org/10.1021/cr980421n.
13. Mao, B.; Calatayud, D. G.; Mirabello, V.; Hodges, B. J.; Martins, J. A. R.; Botchway, S. W.; Mitchels, J. M.; Pascu, S. I. Interactions between an Aryl Thioacetate-Functionalized Zn(II) Porphyrin and Graphene Oxide. *Adv Funct Mater* **2016**, *26* (5), 687–697. https://doi.org/10.1002/adfm.201504147.
14. Ye, T.; Ye, S.; Chen, D.; Chen, Q.; Qiu, B.; Chen, X. Spectroscopic Characterization of Tetracationic Porphyrins and Their Noncovalent Functionalization with Graphene. *Spectrochim Acta A Mol Biomol Spectrosc* **2012**, *86*, 467–471. https://doi.org/10.1016/j.saa.2011.10.070.
15. Wang, Y. Te; Wu, R. R.; Zhang, Y. Y.; Wang, B. H.; Lee, H. W. Photoelectric Conversion Performance of Water-Soluble Palladium–Porphyrin/Graphene Oxide Noncovalent Composites. *J Appl Spectrosc* **2023**, *89* (6), 1254–1261. https://doi.org/10.1007/s10812-023-01492-z.
16. Gacka, E.; Wojcik, A.; Mazurkiewicz-Pawlicka, M.; Malolepszy, A.; Stobiński, L.; Kubas, A.; Hug, G. L.; Marciniak, B.; Lewandowska-Andralojc, A. Noncovalent Porphyrin–Graphene Oxide Nanohybrids: The

PH-Dependent Behavior. *The Journal of Physical Chemistry C* **2019**, *123* (6), 3368–3380. https://doi.org/10.1021/acs.jpcc.8b11374.
17. Hu, S.; Wang, Z.; Gu, Y.; Li, Y.; Jia, Y. Clinical Available Circulating Tumor Cell Assay Based on Tetra(4-Aminophenyl) Porphyrin Mediated Reduced Graphene Oxide Field Effect Transistor. *Electrochim Acta* **2019**, *313*, 415–422. https://doi.org/10.1016/j.electacta.2019.05.039.
18. Miao, W.; Shim, G.; Lee, S.; Lee, S.; Choe, Y. S.; Oh, Y.-K. Safety and Tumor Tissue Accumulation of Pegylated Graphene Oxide Nanosheets for Co-Delivery of Anticancer Drug and Photosensitizer. *Biomaterials* **2013**, *34* (13), 3402–3410. https://doi.org/10.1016/j.biomaterials.2013.01.010.
19. Grinceviciute, N.; Snopok, B.; Snitka, V. Functional Two-Dimensional Nanoarchitectures Based on Chemically Converted Graphene Oxide and Hematoporphyrin under the Sulfuric Acid Treatment. *Chemical Engineering Journal* **2014**, *255*, 577–584. https://doi.org/10.1016/j.cej.2014.06.081.
20. Koczorowski, T.; Rębiś, T.; Szczolko, W.; Antecka, P.; Teubert, A.; Milczarek, G.; Goslinski, T. Reduced Graphene Oxide/Iron(II) Porphyrazine Hybrids on Glassy Carbon Electrode for Amperometric Detection of NADH and L-Cysteine. *Journal of Electroanalytical Chemistry* **2019**, *848*, 113322. https://doi.org/10.1016/j.jelechem.2019.113322.
21. Yaqoob, M. D.; Xu, L.; Li, C.; Leong, M. M. L.; Xu, D. D. Targeting Mitochondria for Cancer Photodynamic Therapy. *Photodiagnosis Photodyn Ther* **2022**, *38*, 102830. https://doi.org/10.1016/j.pdpdt.2022.102830.
22. Tampa, M.; Sârbu, M. I.; Mitran, M. I.; Mitran, C. I.; Dumitru, A.; Benea, V.; Georgescu, S. R. Pain in Photodynamic Therapy. *Journal of Mind and Medical Sciences* **2016**, *3* (1)
23. Li, C.; Cheng, Y.; Li, D.; An, Q.; Zhang, W.; Zhang, Y.; Fu, Y. Antitumor Applications of Photothermal Agents and Photothermal Synergistic Therapies. *Int J Mol Sci* **2022**, *23* (14), 7909. https://doi.org/10.3390/ijms23147909.
24. Shi, D.; Li, Y.; Dong, H.; Li, Y. Graphene-Based Nanovehicles for Photodynamic Medical Therapy. *Int J Nanomedicine* **2015**, 2451. https://doi.org/10.2147/IJN.S68600.
25. Dolmans, D. E. J. G. J.; Fukumura, D.; Jain, R. K. Photodynamic Therapy for Cancer. *Nat Rev Cancer* **2003**, *3* (5), 380–387. https://doi.org/10.1038/nrc1071.
26. Viola, E.; Donzello, M. P.; Sciscione, F.; Shah, K.; Ercolani, C.; Trigiante, G. Tetra-2,3-Pyrazinoporphyrazines with Externally Appended Pyridine Rings. 17. Photosensitizing Properties and Cellular Effects of Zn II Octacationic and Zn II /Pt II Hexacationic Macrocycles in Aqueous Media: Perspectives of Multimodal Anticancer Potentialities. *J Photochem Photobiol B* **2017**, *169*, 101–109. https://doi.org/10.1016/j.jphotobiol.2017.03.005.
27. Pia Donzello, M.; Viola, E.; Giustini, M.; Ercolani, C.; Monacelli, F. Tetrakis(Thiadiazole)Porphyrazines. 8. Singlet Oxygen Production, Fluorescence Response and Liposomal Incorporation of Tetrakis(Thiadiazole)Porphyrazine Macrocycles [TTDPzM] (M = MgII(H2O), ZnII, AlIIICl, GaIIICl, CdII, CuII, 2HI). *Dalton Transactions* **2012**, *41* (20), 6112. https://doi.org/10.1039/c2dt12381a.
28. Haddad, R. E.; Gazeau, S.; Pécaut, J.; Marchon, J.-C.; Medforth, C. J.; Shelnutt, J. A. Origin of the Red Shifts in the Optical Absorption Bands of Nonplanar Tetraalkylporphyrins. *J Am Chem Soc* **2003**, *125* (5), 1253–1268. https://doi.org/10.1021/ja0280933.
29. Mei, Q.; Liu, B.; Han, G.; Liu, R.; Han, M.; Zhang, Z. Graphene Oxide: From Tunable Structures to Diverse Luminescence Behaviors. *Advanced Science* **2019**, *6* (14), 1900855. https://doi.org/10.1002/advs.201900855.
30. Kuznetsova, N. A.; Gretsova, N. S.; Derkacheva, V. M.; Mikhalenko, S. A.; Solov'eva, L. I.; Yuzhakova, O. A.; Kaliya, O. L.; Luk'yanets, E. A. Generation of Singlet Oxygen with Anionic Aluminum Phtalocyanines in Water. *Russ J Gen Chem* **2002**, *72* (2), 300–306. https://doi.org/10.1023/A:1015402524813.

9. ACRONYMS

ADMA - Tetrasodium-9,10-anthracenediyl**-**bis(methylene)malonate

CTC – Circulating Tumor Cells

DFT - Density Functional Theory

DMF - Dimethylformamide

DMSO - Dimethyl Sulfoxide

FT-IR: Fourier Transfrom Infrared Spectroscopy

GO - Graphene Oxide

IR - Infrared

NMR - Nuclear Magnetic Resonance Spectroscopy

PDT - Photodynamic Therapy

PL - Photoluminescence

PS - Polystyrene

PTT - Photothermal Therapy

Pc - Phthalocyanine

Py - Pyridine

Pz - Porphyrazine

Pz@GO – Hybrid Porphyrazine-Graphene Oxide Material

RPE – Extra Pure Reagent

TD-DFT - Time-Dependent Density Functional Theory

UV-Vis: Ultraviolet-Visible

APPENDICES

APPENDIX 1: STABILITY OF PZ@GO IN WATER THROUGH TIME

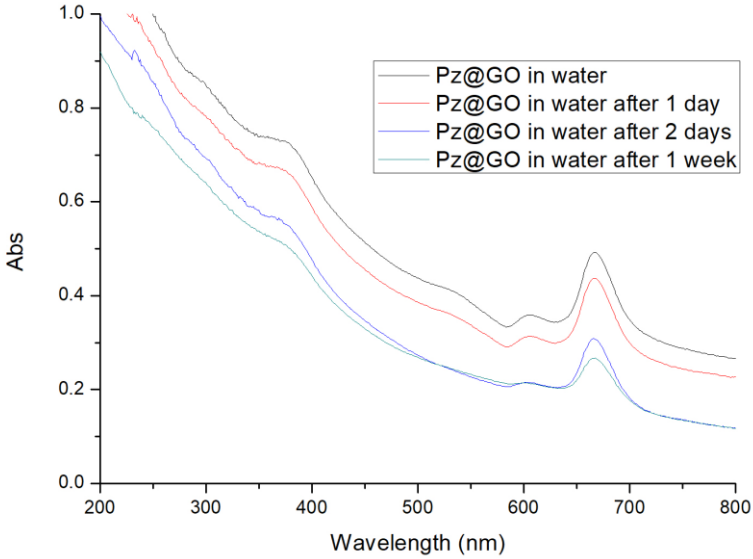

Figure 25. UV-visible spectra of Pz@GO in water after immediately diluting it (black), one day later (red), two days later (blue) and one week later (green).

APPENDIX 2: UV-VISIBLE SPECTRA OF PCALSMIX AND ADMA IN H2O, WITH AN INCREASING AMOUNT OF GO.

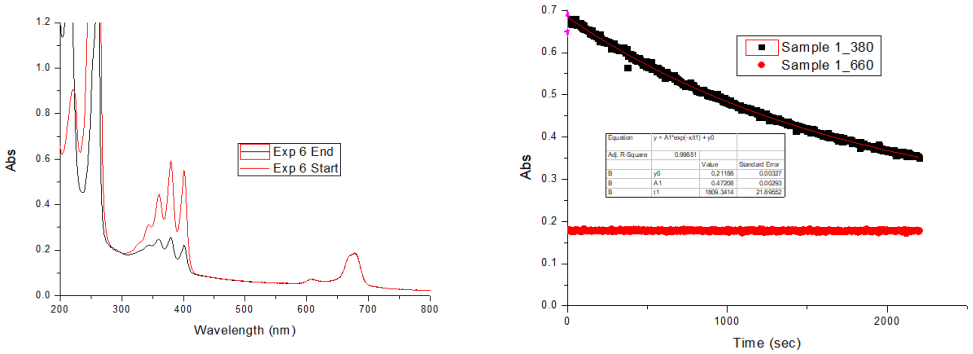

Figure 26. A) UV-visible spectra of $PcAlS_{mix}$ and ADMA in H_2O with the addition of 0.2 mL of GO solution, before (red line) and after (black line) laser irradiation (λ_{irr} = 660 nm); B) Absorbance values indicating ADMA photo-oxidation (red plot) and sensitizer Q-band maximum (dark dots) during irradiation; the related first-order exponential fit (black line) is also shown.

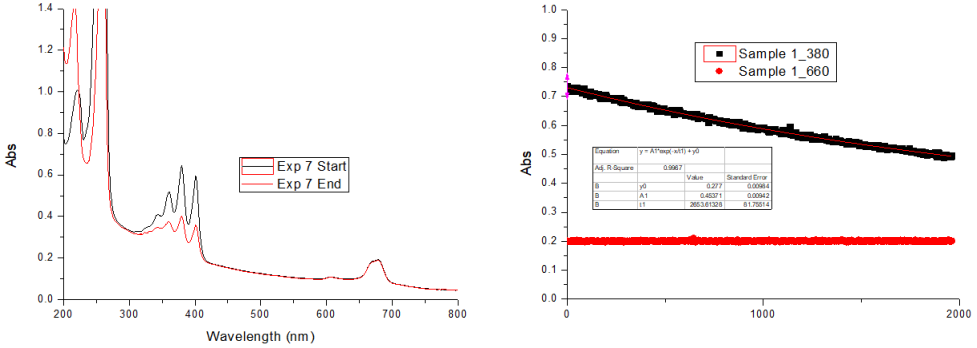

Figure 27. A) UV-visible spectra of $PcAlS_{mix}$ and ADMA in H_2O with the addition of 0.4 mL of GO solution, before (red line) and after (black line) laser irradiation (λ_{irr} = 660 nm); B) Absorbance values indicating ADMA photo-oxidation (red plot) and sensitizer Q-band maximum (dark dots) during irradiation; the related first-order exponential fit (black line) is also shown.

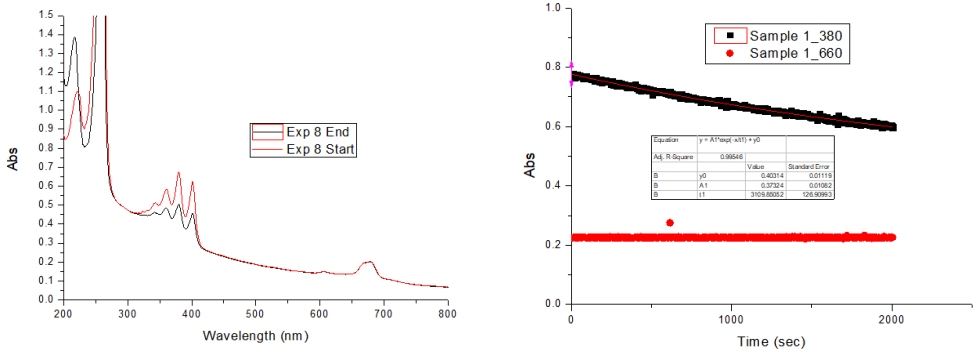

Figure 28. A) UV-visible spectra of $PcAlS_{mix}$ and ADMA in H_2O with the addition of 0.6 mL of GO solution, before (red line) and after (black line) laser irradiation (λ_{irr} = 660 nm); B) Absorbance values indicating ADMA photo-oxidation (red plot) and sensitizer Q-band maximum (dark dots) during irradiation; the related first-order exponential fit (black line) is also shown.